

RSC Advances



This is an *Accepted Manuscript*, which has been through the Royal Society of Chemistry peer review process and has been accepted for publication.

Accepted Manuscripts are published online shortly after acceptance, before technical editing, formatting and proof reading. Using this free service, authors can make their results available to the community, in citable form, before we publish the edited article. This *Accepted Manuscript* will be replaced by the edited, formatted and paginated article as soon as this is available.

You can find more information about *Accepted Manuscripts* in the [Information for Authors](#).

Please note that technical editing may introduce minor changes to the text and/or graphics, which may alter content. The journal's standard [Terms & Conditions](#) and the [Ethical guidelines](#) still apply. In no event shall the Royal Society of Chemistry be held responsible for any errors or omissions in this *Accepted Manuscript* or any consequences arising from the use of any information it contains.

ARTICLE

Surface modification of TiO₂ by ionic liquid electrolyte in dye-sensitized solar cells using a molecular insulator

Cite this: DOI: 10.1039/x0xx00000x

Received 00th January 2012,
Accepted 00th January 2012

DOI: 10.1039/x0xx00000x

www.rsc.org/

Molang Cai^{b,c}, Xu Pan^{c*}, Weiqing Liu^c, John Bell^b, and Songyuan Dai^{a*}

A factor that limits the performance of dye-sensitized solar cell (DSC) based on ionic liquid is the disappearance of electron density due to electron recombination at the Dyed-TiO₂/electrolyte interface. Adding an additive to the electrolyte can affect processes related to kinetics of the electron recombination. In this paper a novel solid state additive, 1,2-dimethylimidazolium-3-propylsulfonate (DMImBS), was synthesized by autoclave and directly applied to a DSC based on an ionic liquid electrolyte to form a molecular insulator layer. It was found that the presence of DMImBS in the ionic liquid electrolyte enhances both the open circuit photovoltage (V_{oc}) and fill factor (FF) without significant penalty in photocurrent (J_{sc}), as well as significantly increasing the power output of the DSC. This is suggested to be mainly due to the passivation of surface states, which effectively reduces electron recombination and restrains the Li⁺ intercalation. The device based on DMImBS also showed outstanding stability under prolonged light soaking at 50 °C, maintaining 100% photovoltaic efficiency.

1. Introduction

Dye sensitized solar cells (DSC) attract immense attention in scientific research and industrial applications as low production cost solar cells¹⁻⁴. Three components are generally present in DSC: a nanocrystalline mesoporous TiO₂ thin film coated on a conducting glass substrate with a monolayer of dye as a sensitizer, an electrolyte containing I⁻/I₃⁻ and a platinum counter electrode. Electrons generated by photo-excited dye molecules are injected into the conduction band of the TiO₂ and transported from the injection sites to the contact electrode under light irradiation. Finally, electrons are collected at the transparent conducting glass substrate interface and then pass through the external circuit. It is believed that electron transfer at the Dyed-TiO₂/electrolyte interfaces and redox charge transfer at the counter electrode plays an important role in determining the photovoltaic performances of DSC⁵. Additives

in the electrolyte can affect processes related to kinetics of the electron transport and recombination, for this reason studies have been made on additives to improve the DSC efficiency and stability⁶⁻¹².

Electron transfer dynamics at the Dyed-TiO₂/electrolyte interface is the key factor effecting the short circuit photocurrent (J_{sc}) and open circuit photo voltage (V_{oc}), which is related to photoelectric conversion efficiency (η)¹³⁻¹⁷. Various additives have been added to the electrolyte solution, such as 4-tert-butylpyridine (TBP)^{18,19}, N-methylbenzimidazol (NMBI), benzimidazol (BI)^{20,21} and lithium iodide (LiI)^{22,23}, to improve the device efficiency. To the best of our knowledge, adsorption of TBP, NMBI or BI on the TiO₂ surface can elevate the conduction band edge (V_{CB}) of TiO₂ to increase V_{oc} ²⁴. Raising V_{CB} would also decrease the electron injection efficiency (η_i)

and explain the reduced J_{sc} observed in DSC using these additives^{25,26}. The electron transfer is improved by laying Li^+ in the TiO_2 crystal. In addition, the presence of LiI causes a positive shift in the V_{CB} of TiO_2 which explains the increase in J_{sc} and decrease in V_{oc} ²⁷.

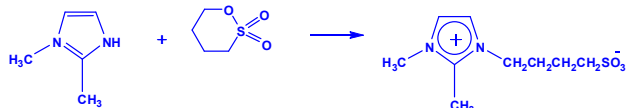
Electrolyte, as the redox mediators transport layer, is an important component in DSC. Organic solvents, such as γ -butyrolactone, acetonitrile and 3-methoxypropionitrile, are conventionally used as DSC electrolyte solvents but they are usually poisonous and volatile, which results in the restriction of DSC industrialization. The air and water stable room temperature ionic liquids (RTILs) are attractive as solvents due to their chemical and thermal stability, negligible vapor pressure, nonflammability, high ionic conductivity and wide electrochemical window²⁸. Furthermore, the physical and chemical properties of RTILs can be changed by varying the nature of cations and anions. During past decades, ionic liquid electrolytes based on imidazolium compounds have been applied in DSC but η is still lower than when organic solvent electrolytes are used. Some works reported that electron recombination is more apparent using ionic liquid electrolyte compared to using organic solvent electrolyte^{29,30}, however it is necessary to find a more effective additive to restrain the electron recombination in DSC based on ionic liquid electrolyte.

Recently, large efforts have been made to select and prepare new materials in order to achieve higher performance in DSC. In this paper, we report on the characterization of a zwitterionic imidazolium propylsulfonate, 1,2-dimethylimidazolium-3-propylsulfonate (DMImBS), as a novel solid state additive in 1-methyl-3-propylimidazolium iodide (MPII) based electrolyte. The alkyl chain of DMImBS is suggested to form the insulation layer which restrains the electron recombination and intercalation of Li^+ . The negligible vapor pressure of DMImBS as a solid material is good for the stability of DSC.

2. Experimental

2.1 Materials

Anhydrous lithium iodide, 1,2-dimethylimidazole, and 1,4-butanediol were purchased from Aldrich and used as received. The synthesis of zwitterionic-type salt having an imidazolium cation is shown below in scheme 1^{31,32}. Their structures were confirmed by 1H-NMR spectroscopy (Bruker DMX 400 spectrometer using D_2O as solvents).



Scheme 1 Synthesis and characterization of 1,2-dimethylimidazolium-3-propylsulfonate (DMImBS)

The mixture of 1,2-dimethylimidazole (9.61 g, 0.1 mol) and 1,4-butanediol (13.62 g, 0.1 mol) was placed in a 60 mL Teflon-lined, stainless steel autoclave, and was heated in an oven at

100 °C for 7 h. The resulting DMImBS was decanted and dried under vacuum at 70 °C for 6 h. Crude products were washed with 1,1,1-trichloroethane before drying, using a weight ratio of 1:2 for crude products to 1,1,1-trichloroethane. 1 H NMR spectra of DMImBS were measured on a Bruker DMX 300 spectrometer using D_2O as solvent. 1H-NMR (D_2O , 400MHz): δ 1.59 (m, 2H), 1.79 (m, 2H), 2.42 (s, 3H), 2.78 (t, 2H), 3.59 (s, 3H), 4.00 (t, 2H), 7.15 (s, 1H), 7.20 (s, 1H).

The standard electrolyte (electrolyte A) contains 0.1 mol/L iodine (I_2 , 99%, Aldrich) and 0.1 mol/L anhydrous lithium iodide (LiI , 99%, Aldrich) dissolving in MPII. To prepare electrolyte B and electrolyte C, 0.2 mol/L DMImBS and 0.5 mol/L TBP was added into the standard electrolyte, respectively. Electrolyte A, electrolyte B and electrolyte C were used to assemble Device A, Device B and Device C, respectively.

2.2 DSC assembly

TiO_2 (anatase) colloidal solution was prepared by hydrolysis of titanium tetraisopropoxide³³. The TiO_2 paste was printed on transparent conducting glass sheets (TEC-15, LOF) and sintered in air at 450 °C for 30 min. The film was 10 μm thick, which was determined by a profilometer (XP-2, AMBIOS Technology Inc. USA). A 4- μm -thick light scattering layer was used. After cooling to 80 °C, the TiO_2 films were immersed in an anhydrous ethanol solution with 5.0×10^{-4} M cis-dithiocyanate-N,N'-bis-(4-carboxylate-4-tetrabutylammonium carboxylate-2,2'-bipyridine) ruthenium (II) (N719) for 12 h. Excess N719 dye in TiO_2 films was rinsed off with anhydrous ethanol before assembly. The counter electrode was platinized using H_2PtCl_6 solution on transparent conducting glass and fired in air at 410 °C for 20 min. Then, it was placed directly on the top of the dye-sensitized TiO_2 films. The gap between the two electrodes was sealed by thermal adhesive (Surlyn, Dupont). The electrolyte was then filled from a hole made on the counter electrode and the hole was later sealed by a cover glass and thermal adhesive films. The total active electrode area of the DSC was 0.25 cm^2 .

2.3 Measurements

The adsorption process of DMImBS was investigated by fourier transform infrared spectroscopy (FTIR). Electrochemical impedance spectroscopy (EIS) is performed to investigate the electron recombination at the Dyed- TiO_2 /electrolyte interface modified with and without DMImBS. The photovoltaic performances of DSC were measured with a Keithley 2420 digital source meter (Keithley, USA), under a 450 W Xenon lamp (Oriel, USA) with a filter (AM 1.5). Electrochemical impedance spectroscopy (EIS) measurements were carried out on IM6ex (Germany, Zahner Company), at perturbation amplitude of 5 mV within the frequency range from 3 MHz to 5 mHz in the dark. Intensity modulate photocurrent spectroscopy and intensity modulate photo voltage spectroscopy (IMVS/IMPS) measurements were also performed on an IM6ex using light emitting diodes ($\lambda=610$ nm) driven by Export (Germany, Zahner Company). The LED provided both *dc* and

ac components of the illumination. A small *ac* component is 10% or less than that of the *dc* component and the frequency range was 3 kHz to 0.3 Hz. The IR spectra for all the samples were measured using a NICOLET8700 FTIR spectrometer (USA, Thermo Fisher Scientific). The Raman spectra were measured by LABRAM-HR (Franch, YJ).

The samples for ATR-FTIR and UV-vis were prepared by immersing TiO₂ films (5 μm) in a 0.2 mol/L DMImBS glycol solution (DMImBS/TiO₂) and a 0.5 mmol/L N719 ethanol solution (N719/TiO₂) for 12 h respectively. These samples were then rinsed with ethanol three times and dried under vacuum at room temperature. Thereafter, one of the Dyed-TiO₂ films was dipped into the 0.2 mol/L DMImBS glycol solution for 12 h (DMImBS/N719/TiO₂). The coated film was then rinsed with glycol and dried under vacuum at room temperature.

The DMImBS/TiO₂ sample for Raman spectra were prepared by immersing TiO₂ powder in a 0.2 mol/L DMImBS glycol solution for 12 h, then rinsed with ethanol three times and dried under vacuum at room temperature.

3. Results and Discussion

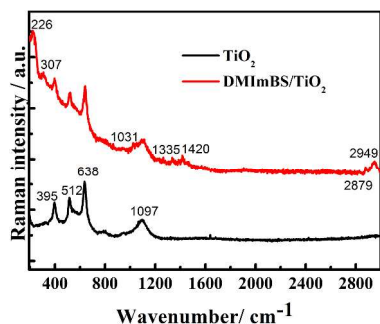


Figure 1. The FT-Raman spectra of TiO₂ and DMImBS/TiO₂.

Figure 1 shows the Raman spectra of TiO₂ and DMImBS/TiO₂. The anatase TiO₂ has Raman-active fundamentals in the vibrational spectrum. The peaks at 638 cm⁻¹, 395 cm⁻¹ and 512 cm⁻¹ are attributed to E_g mode, B_g mode and A_g mode respectively. In the high wavenumber region of the Raman spectrum of DMImBS/TiO₂ sample, new bands are obtained at 2879 cm⁻¹ and 2949 cm⁻¹ which are assigned to the C–H stretching of the methyl and methylene groups.^{34,35} Imidazolium ring stretching modes give rise to weak bands at 1420 cm⁻¹ and 1335 cm⁻¹.³⁶ The peaks at 226 cm⁻¹ and 307 cm⁻¹ are assigned to ω(N–C) and bending vibration of imidazolium.³⁷ The symmetric stretching mode of SO₃⁻¹ is between 1025 and 1080 cm⁻¹, this peak is observed at 1031 cm⁻¹ for DMImBS.³⁸ The result indicate that DMImBS adsorb on the TiO₂ surface.

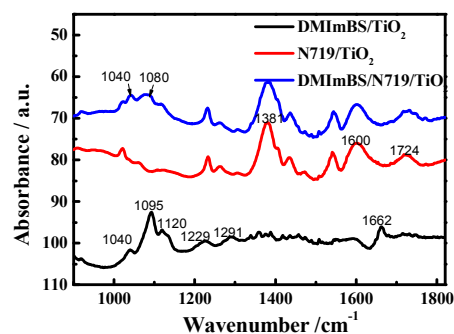


Figure 2. ATR-FTIR spectra of DMImBS/TiO₂, N719/TiO₂ and DMImBS/N719/TiO₂. All of the ATR-FTIR spectra of samples on the TiO₂ film were obtained by subtracts the blank TiO₂ film sample.

The ATR-FITR spectra of DMImBS/TiO₂, N719/TiO₂ and DMImBS/N719/TiO₂ films are compared in Figure 2. The band at 1229 cm⁻¹ and 1291 cm⁻¹ are attributed to asymmetric sulfonyl (O=S=O) stretching vibrations of the sulfonate groups (ν_{as} (R-SO₃⁻)). 1120 cm⁻¹ and 1040 cm⁻¹ can be assigned to symmetric sulfonyl stretching vibrations (ν_s (R-SO₃⁻)).³⁹ Sulfonate groups are very sensitive to changes in local coordination geometry; a symmetry change of sulphate and sulfonate groups may result in splits or shifts in the asymmetric vibrations⁴⁰. The spectra of DMImBS/TiO₂ samples predict that adsorption of DMImBS on the TiO₂ surface occurs. Comparison of DMImBS/N719/TiO₂ with DMImBS/TiO₂ shows that the intensity of the ν_{as} (R-SO₃⁻) band is diminished relative to other bands when co-adsorption with N719 is added. The change upon adsorption to TiO₂ surface is suggested to be due to a change in the local environment of the sulfonate head⁴¹. Kevin⁴² reported that the adsorbed surfactant was surface-bound via electrostatic and hydrogen bonding interactions between the sulfate head group and the oxide surface. In the DMImBS/TiO₂ sample, small peaks between 1400 cm⁻¹ and 1550 cm⁻¹ are assigned to ν (C=N) of imidazole group. The band at 1662 cm⁻¹ is attributed to ν (C=C). The ν (C=N) peak of imidazole group is observed in the DMImBS/N719/TiO₂ sample.^{43,44} Due to the weak electrostatic adsorption between imidazolium cation and TiO₂ surface, the intensity of characteristic peak is very weak. From the IR spectroscopic data we further confirm that the DMImBS adsorbed on the TiO₂ surface and the sulfonate group is predominant adsorption group^{45,46}.

The N719/TiO₂ shows strong bands at 1600 cm⁻¹ and 1381 cm⁻¹, due to ν_{as} (-COO⁻) and ν_s (-COO⁻), which are attributed to the carboxylate group anchored to the TiO₂ surface. The bands at 1724 cm⁻¹ are due to the ν (C=O) and ν (C-O) of the free carboxylic acid of N719⁴⁷⁻⁴⁹. The intensity at 1724 cm⁻¹ relative to that at 1381 cm⁻¹ indicates the relative amounts of unstable and stable type dye molecules on the TiO₂ surface⁵⁰. The intensity of these characteristic peaks do not significantly change between the N719/TiO₂ and DMImBS/N719/TiO₂ 0, which indicates that dye adsorption is not influenced by co-adsorption with DMImBS.

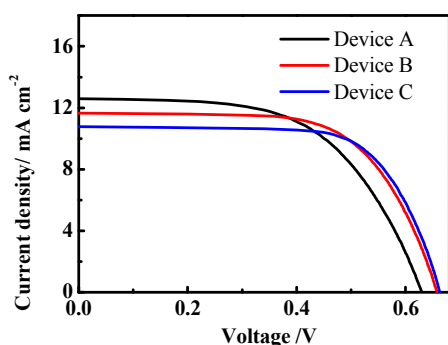


Figure 3. Current density-voltage characteristics of Device A, Device B and device C under AM 1.5 simulated sunlight (100 mW cm^{-2}) illumination.

Table 1 The I - V parameters of Device A, Device B and Device C, the active area is 0.25 cm^2 controlled by a black mask.*

Device	V_{oc}/V	$J_{sc}/\text{mA cm}^{-2}$	FF	$\eta/\%$
A	0.63 ± 0.01	12.35 ± 0.44	0.57 ± 0.02	4.42 ± 0.12
B	0.66 ± 0.00	11.28 ± 0.35	0.65 ± 0.01	4.83 ± 0.08
C	0.67 ± 0.00	10.29 ± 0.44	0.67 ± 0.02	4.62 ± 0.09

*The results are the average values obtained from 5 cells with standard deviation.

I - V curves of Device A, Device B and Device C measured under full air mass 1.5 AM (intensity of the solar simulator: 100 mW/cm^2) are predicted in Figure 3. The J_{sc} , V_{oc} and fill factor (FF) of Device A are 12.56 mA cm^{-2} , 0.63 V and 0.57 , respectively, yielding an overall the photovoltaic conversion efficiency (η) of 4.53% . The corresponding I - V parameters of Device B with DMImBS as additive are 11.68 mA cm^{-2} , 0.66 V , 0.64 and 4.93% . Table 1 illustrates the average characteristic performance parameters of the DSCs with standard deviation based on five cells of different electrolyte. In general, compared with Device A, Device B has a higher V_{oc} and FF . Using DMImBS as an additive enhances the power conversion efficiency without significant penalty in photocurrent. In addition, Device B containing DMImBS displays better η compared to Device C containing TBP as a classic additive.

DSC is a multi-phase complicated photo-electrochemical system where two phases inside the cell contact each other to form several interfaces. Photoelectric energy conversion of DSC's is related to the processes of electron transfer that take place on the contact interfaces⁵¹. EIS is a powerful frequency-domain technique used to identify and study the kinetics of interface electron transfer in DSC. EIS measures the current response to a modulated applied bias superimposed on a constant applied voltage, it can be evaluated using resistance and capacitance elements as an equivalent circuit. At the Dyed-TiO₂/electrolyte interface electrons are transferred to the electrolyte to react with I_3^- , the difficulty of this reaction can be

denoted with a reaction resistance (R_{ct}). The capacitance of TiO₂ film can be denoted with a chemical capacitance (C_{μ}). The Dyed-TiO₂/electrolyte interface can therefore be represented by a composite component in which R_{ct} is connected in parallel with C_{μ} . Near the counter electrode/electrolyte interface a double electrode layer is formed between the counter electrode surface and the electrolyte, so transfer impedance in the reaction between the electrons and the electrolyte can also be denoted with a composite component consisting of parallel circuit. The R_{CE} is connected in parallel with C_p . By fitting the measurement impedance data, electron transfer resistance and capacitance at the Dyed-TiO₂/electrolyte and the counter electrode/electrolyte interface can be deduced. The fitting results of EIS measurements under various applied potential at equal intervals are plotted in Figure 4.

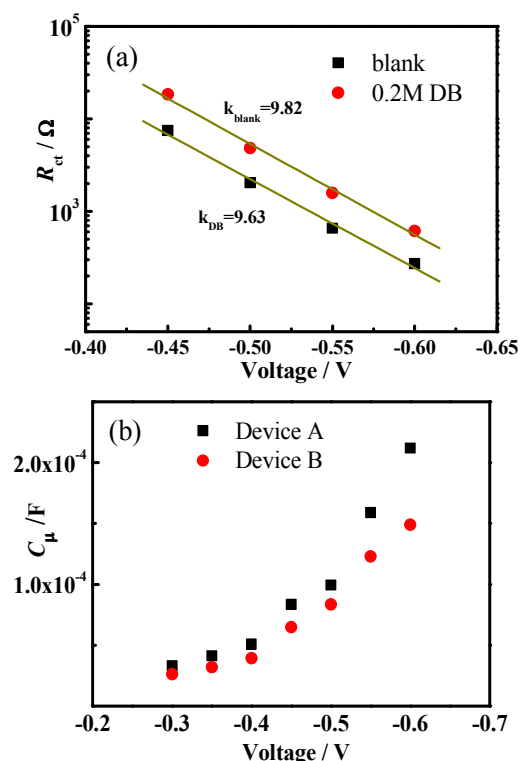


Figure 4 Fitting results (a) recombination resistance (R_{ct}) and (b) chemical capacitance (C_{μ}) of the Nyquist plot obtained from EIS measurements at different applied potential in the dark.

Figure 4 (a) shows that R_{ct} following an exponential decrease going towards negative biases. The values of R_{ct} can be evaluated using Equation (1)^{52,53}

$$R_{ct} = R_0 \exp\left(-e \frac{\beta V}{k_B T}\right) \quad (1)$$

where R_0 is constant, e is the electron charge, V is the bias voltage, k_B is the Boltzmann constant, T is the temperature and β is the transfer coefficient which corresponds to the reciprocal value of diode quality factor. Comparison of device A and device B shows that R_{ct} increases when DMImBS is added to the electrolyte. The V_{oc} is determined by the difference between

the electron quasi-Fermi level in the TiO₂ film under illumination and the redox potential of the electrolyte in the dark. In DSC, photoelectrons easily transfer from the TiO₂ film to the electrolyte and recombine with I₃⁻. Electron recombination plays a significant role in reducing the electron density in the TiO₂ film, a problem which becomes more prevalent when using ionic liquid electrolytes instead of liquid electrolytes²⁶. The increase of R_{ct} indicates that suppression of electron recombination occurs as a means of increasing electron density. This result indicates that addition of DMImBS is effective in retarding the back reaction between I₃⁻ and electrons in TiO₂ film.

Due to the small radius of TiO₂ particles, there is no space charge layer in the nanoporous TiO₂ film. Research shows that the TiO₂ film has two main types of capacitance: chemical capacitance inside the film and Helmholtz double electric layer capacitance at the interface of Dyed-TiO₂/electrolyte (significant only under high bias voltage)⁵⁴⁻⁵⁶. The capacitance of TiO₂ film can be denoted with C_{μ} which is related to the concentration of electrons and the chemical potential of the TiO₂ film⁵⁷. Figure 4 (b) shows a strong exponential increase of C_{μ} with increasing carrier density or bias voltage in the solar cell.

More efforts of electron recombination achieve by the EIS results. the kinetics of electron transfer to I₃⁻ are usually discussed in terms of the electron lifetime (τ_n)⁵⁸, which can be calculated directly from EIS response ($\tau_n = R_{ct} \times C_{\mu}$). The greater τ_n gets, the slower the recombination between electrons and I₃⁻ will be. As shown in Figure 5, at the identical electron energy levels, Device B has a consistently longer apparent recombination lifetime τ_n than that of Device A; further supporting evidence that slower charge recombination occurs in Device B relative to Device A. It is generally believed that electrons may undergo recombination reactions with I₃⁻ on the Dyed-TiO₂/electrolyte interface through the following two ways: direct recombination via conduction band or recombination via surface states. If electrons undergo recombination reactions via the TiO₂ conduction band, β should equal to 1⁵⁹. The values of β are 0.24 for both Device A and Device B, which is calculated from the slope of the straight line as illustrated in Figure 4(a). Both values of β are less than 1, indicating that electrons primarily undergo recombination reactions via the surface state rather than via the TiO₂ conduction band. Since DMImBS only covers the surface of the TiO₂, it can be inferred that electron recombination via surface state may play an importance role in DSC.

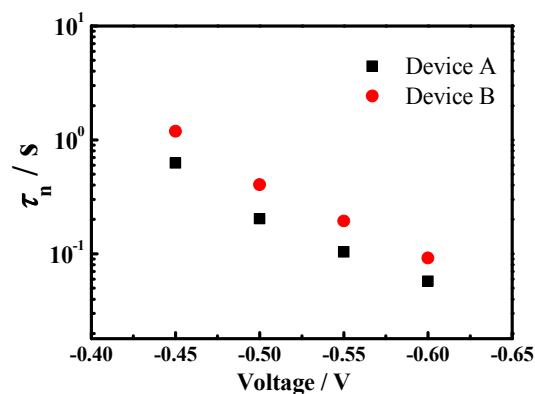


Figure 5 The lifetime versus applied potential in Device A and Device B.

To further investigate the kinetics of electron transfer at the Dyed-TiO₂/electrolyte interface are generally discussed according to the results of IMVS/IMPS measurements. The V_{oc} of DSC are dependent on the gap between the TiO₂ Fermi energy level and the redox potential in the electrolyte. As shown in Figure 6, lithium perchlorate (LiClO₄) is used as the lithium salts in the electrolyte, and the redox potentials in each electrolyte are maintained throughout the experiment with the same I⁻/I₃⁻ ratio. Improvement of the V_{oc} therefore depends on the suppression of recombination and the TiO₂ conduction band shift, they are both related to TiO₂ Fermi energy level. As we know, a major feature of nano porous TiO₂ film is that a large number of excess electrons can be stored within the network. The charge buildup on the surface of TiO₂ particles causes the variation of potential across the Helmholtz layer, resulting in the TiO₂ conduction band edge movement¹⁸. Positive charge buildup causes the band edges to shift downward toward positive electrochemical potentials, which leads to the decrease in V_{oc} . The difference between the TiO₂ conduction band edge and the quasi-Fermi level depends on the photo induced charge (Q)⁵⁵. For a given Q , the increase in V_{oc} is attributed to an upward shift of the TiO₂ conduction band whereas a decrease in V_{oc} is attributed to a downward shift of the TiO₂ conduction band. Figure 6 (a) depicts the dependence of V_{oc} on $\ln(Q)$ in TiO₂ at open circuit following Equation (2)¹⁸

$$V_{oc} = V_0 + m_0 \ln Q \quad (2)$$

where V_0 is the vertical intercept and m_0 is the slope rate, that is, $m_0 = dV_{oc}/d \ln Q$.

Along with the increase of LiClO₄ consistency in the electrolyte, the TiO₂ conduction band shows a gradual positive shift and decrease in V_{oc} at constant Q . Adsorption of Li⁺ on the TiO₂ surface leads to a positive shift of the TiO₂ conduction band potential⁶⁰. Employing DMImBS alone as an additive negatively shifts the conduction band and increases the V_{oc} slightly at constant Q . As previously mentioned in the IR data, sulfate is the major adsorption group, anchoring to the TiO₂ surface. The conduction band shift is suggested to be due to the negative charge of sulfate. Moreover, addition of DMImBS in the electrolyte containing LiClO₄ causes an obviously upward

shift of the TiO₂ conduction band. The conduction bands shift back to the negative potential is attributed to a reduction in the amount of adsorbed Li⁺ on the TiO₂ surface.

Due to the small size of TiO₂ particles and effect of electrolyte shielding, the driving force for electron transport in the TiO₂ film is the electron concentration gradient in film, but not electric field action⁶¹. The electron transit time (τ_d) is associated with electron transport in porous TiO₂ film, which can be obtained directly from IMPS⁶². The relation between τ_d and J_{sc} can be described following the exponential distribution in Equation (3)⁶³

$$\tau_d \propto J_{sc}^{\alpha-1} \quad (3)$$

where the parameter α is related to the steepness of the trap-state distribution. As predicted in Figure 6 (b), τ_d is a function of the J_{sc} in double logarithmic form and τ_d decrease with the increase of the J_{sc} in devices. At the constant of J_{sc} , the τ_d of device with LiClO₄ slightly increases when compared with the device without additive. In the presence of the DMImBS, TiO₂ conduction band undergoes a negative shift, which harms the electron injection. The condition of grain boundaries between TiO₂ particles can influence electron transport⁶⁴, DMImBS molecules cover the surface of joints between TiO₂ particles, hindering the electron transport and thus increasing τ_d . The slope of the $\ln(\tau_d)$ versus $\ln(J_{sc})$ plot, which reflects the trap-state distribution of TiO₂ surface, is described by α in Equation (3)⁶⁵. The decrease of α is ascribed to the widening of the exponential conduction band and corresponds to a steeper trap state distribution, which may slow down the electron transport process⁶⁶. The values of α are 0.56, 0.56, 0.51, 0.58 and 0.55 for the X1, X2, X3, X4 and X5, respectively. The steeper trap state distribution with addition of LiClO₄ is attributed to the Kopidakis et al. reported that the Li⁺ intercalated into TiO₂ electrodes⁶⁷. However, the trap state distribution obviously gets shallow with addition of DMImBS, even with the concentration increase of LiClO₄. Trap state distribution doesn't change with presence of DMImBS alone. So the variety of trap state distribution is not directly derived from adsorption of DMImBS on the surface. There should be some interaction between Li⁺ and DMImBS. We presumed that the addition of DMImBS restrain the intercalation of Li⁺ and improve the cell stability in the aging process.

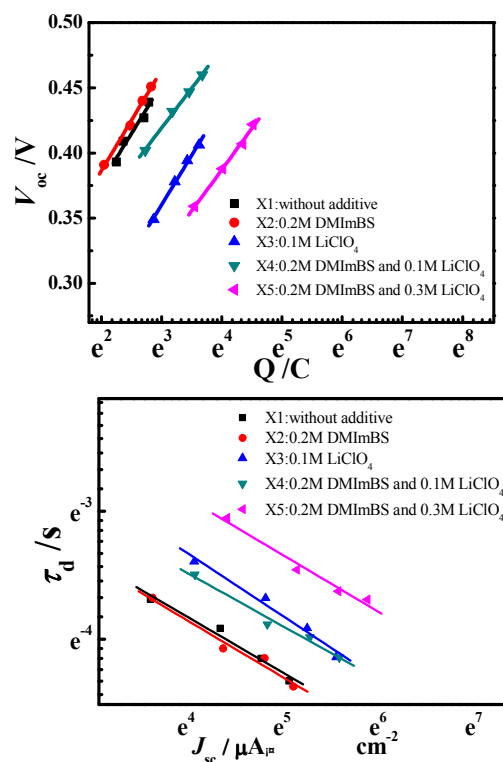


Figure 6 Relationship between (a) V_{oc} and Q (b) τ_d and Q in different devices with various additive.

The counter electrode is an equally important component of DSC. Normally, fluorine-doped tin oxide glass is coated with platinum to afford more reversible electron transfer. The counter electrode/electrolyte interface is a catalytic interface and its role is to transfer electrons arriving from the external circuit back to the electrolyte. The R_{CE} is an important parameter for the performance of DSC, and it depends on the electrochemical reaction rate at the counter electrode/electrolyte interface. The capacitance of the counter electrode/electrolyte interface can be denoted by a Helmholtz double electric layer capacitance^{56,68,69}. Figure 7 presents the R_{CE} and C_p of Device A and Device B at the counter electrode/electrolyte interface. At a given dark current, there are very small differences of R_{CE} and C_p between Device B and Device A. This result rules out the effect from the electron transfer process occurring at the counter electrode with DMImBS. In other words, DMImBS does not influence the catalytic activity of the counter electrode/electrolyte interface.

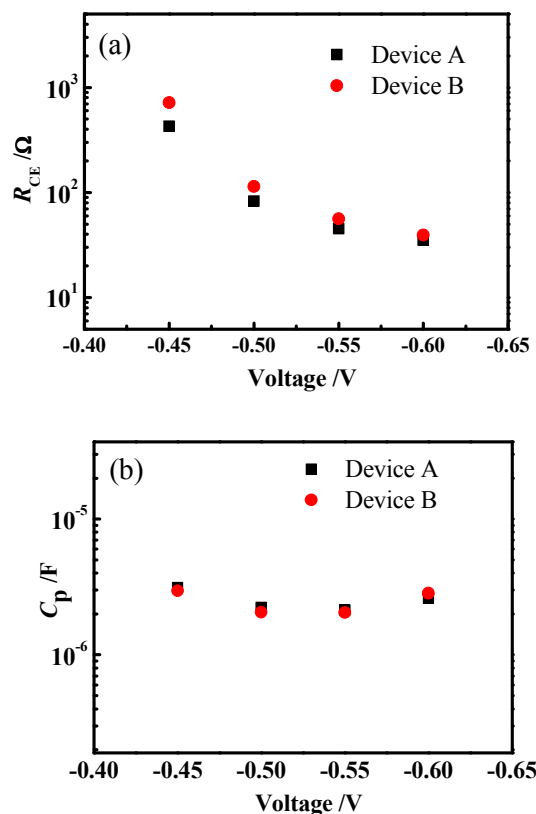


Figure 7 Results of EIS measurements with cells made by nanoporous TiO_2 films in the absence and presence of DMImBS at the counter electrode/electrolyte interface. (a) Electron transfer resistance R_{CE} and (b) capacitance C_p at different applied potential in the dark.

For practical use of DSC, long-term stability of the solar cell is essential. Studies showed that the process of electron transfer at the Dyed- TiO_2 /electrolyte interface increases during the aging process of DSC based on ionic liquid electrolyte⁷⁰. This is a main cause of performance decrease in DSC so keeping the Dyed- TiO_2 /electrolyte interface stable is still a challenging task. Figure 8 shows the photovoltaic parameter evolution of Device A, Device B and Device C during the accelerated experimental conditions in the solar simulator covered by an ultraviolet absorbing polymer film at 50 °C for 1000 h. η of Device B remains stable during the long-term accelerated aging tests, however, the η of Device A and C decrease during the aging process. This may be due to DMImBS adsorption forming a more stable Dyed- TiO_2 /electrolyte interface, leading to long term stability. The J_{sc} , V_{oc} and FF during aging process are provided as shown in the picture. During the aging time, the J_{sc} value goes down, but the device with the DMImBS (Device B) is better than other two. The V_{oc} of device B almost maintains the same level, and the FF obviously goes up compared to the other two device. The major factor of efficiency improvement is increase of FF .

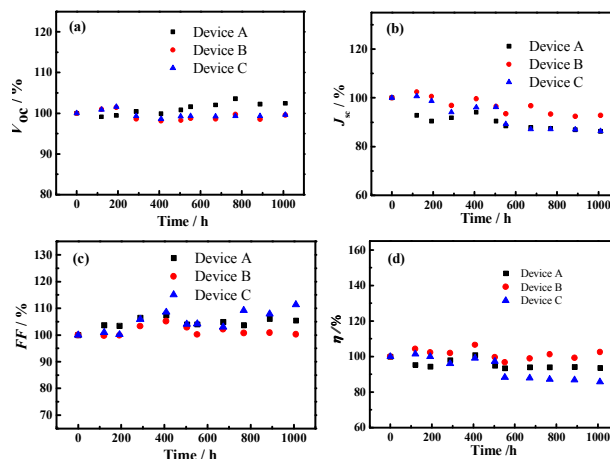


Figure 8 Temporal evolution of photovoltaic parameters (a) V_{oc} (b) J_{sc} (c) FF (d) η of Device A, Device B and Device C during successive one sun light soaking with UV cut-off filter at 50 °C in 1000 h. (Data values have been normalized)

Conclusions

In conclusion, we have identified DMImBS as a novel solid additive which can improve performance of DSC based on ionic liquid electrolyte. DMImBS successfully adsorbed on TiO_2 surface when DMImBS was added to MPlI-based ionic liquid electrolyte. The alky fridge is formed with two functional group adsorption. The electron recombination is effectively restrained by the DMImBS modification. Adsorption of dye molecular was not influenced by the co-adsorption of DMImBS. The intercalation of Li^+ in TiO_2 film was restrained by the adsorption of DMImBS. Therefore, modification of the interface improved the stability of solar cell. The V_{oc} and FF of the DSC were significantly improved without significant decrease in J_{sc} . Use of DMImBS as an additive substantially increased the power output of the DSC due to suppression of interfacial recombination, whilst achieving a more stable interface which improves long-term stability of the DSC.

Acknowledgements

This work is financially supported by the National Basic Research Program of China under Grant No. 2011CBA00700, the National High Technology Research and Development Program of China under Grant No. 2010AA050510, National Natural Science Foundation of China (Grant No. 21103197) and National Natural Science Foundation of China (Grant No. 21173227).

Notes and references

^a State Key Laboratory of Alternate Electrical Power System with Renewable Energy Sources, North China Electric Power University, Beijing, 102206, P. R. China

^b School of Chemistry, Physics and Mechanical Engineering, Queensland University of Technology, Brisbane, QLD 4001, Australia.

- ^c Division of Solar Energy Materials and Solar Cells, Institute of Plasma Physics, Chinese Academy of Sciences P.O.Box:1126, Hefei, Anhui, P. R. China
- ^d Key Laboratory of Nondestructive Testing, Ministry of Education, School of the Testing and Photoelectric Engineering, Nanchang Hangkong University, Nanchang 330063, P. R. China
- *Corresponding Author
sydai@ncepu.edu.cn
mars_dark@hotmail.com
1. S. Mathew, A. Yella, P. Gao, R. Humphry-Baker, F. E. Curchod, N. Ashari-Astani, I. Tavernelli, U. Rothlisberger, K. Nazeeruddin and M. Grätzel, *Nat Chem*, 2014, **6**, 242-247.
 2. D. Sabba, S. Agarwala, S. Pramana and S. Mhaisalkar, *Nanoscale Research Letters*, 2014, **9**, 1-9.
 3. C.-L. Lee, W.-H. Lee and C.-H. Yang, *Journal of Materials Science*, 2013, **48**, 3448-3453.
 4. M. Gratzel, *Nature*, 2001, **414**, 338-344.
 5. M. K. Nazeeruddin, F. De Angelis, S. Fantacci, A. Selloni, G. Viscardi, P. Liska, S. Ito, B. Takeru and M. G. Gratzel, *Journal of the American Chemical Society*, 2005, **127**, 16835-16847.
 6. D. Xu, X. Chen, L. Wang, L. Qiu, H. Zhang and F. Yan, *Electrochimica Acta*, 2013, **106**, 181-186.
 7. M.-J. Kim and N.-G. Park, *Applied Surface Science*, 2012, **258**, 8915-8918.
 8. S. Raja, C. Satheeshkumar, P. Rajakumar, S. Ganesan and P. Maruthamuthu, *Journal of Materials Chemistry*, 2011, **21**, 7700-7704.
 9. K. Hara, Y. Dan-oh, C. Kasada, Y. Ohga, A. Shinpo, S. Suga, K. Sayama and H. Arakawa, *Langmuir*, 2004, **20**, 4205-4210.
 10. M. K. Nazeeruddin, A. Kay, I. Rodicio, R. Humphry-Baker, E. Mueller, P. Liska, N. Vlachopoulos and M. Gratzel, *Journal of the American Chemical Society*, 1993, **115**, 6382-6390.
 11. P. Wang, Q. Dai, S. M. Zakeeruddin, M. Forsyth, D. R. MacFarlane and M. Grätzel, *Journal of the American Chemical Society*, 2004, **126**, 13590-13591.
 12. S. Chang, K. Y. Wong, X. Xiao and T. Chen, *RSC Advances*, 2014, **4**, 31759-31763.
 13. M. Cai, X. Pan, W. Liu, J. Sheng, X. Fang, C. Zhang, Z. Huo, H. Tian, S. Xiao and S. Dai, *Journal of Materials Chemistry A*, 2013, **1**, 4885-4892.
 14. Z. Liang, W. Liu, J. Chen, L. Hu and S. Dai, *ACS Applied Materials & Interfaces*, 2014, **7**, 1100-1106.
 15. M. Xiao, F. Huang, W. Xiang, Y.-B. Cheng and L. Spiccia, *Journal of Power Sources*, 2015, **277**, 343-349.
 16. E. Palomares, J. N. Clifford, S. A. Haque, T. Lutz and J. R. Durrant, *Journal of the American Chemical Society*, 2003, **125**, 475-482.
 17. R. Hou, S. Yuan, X. Ren, Y. Zhao, Z. Wang, M. Zhang, D. Li and L. Shi, *Electrochimica Acta*, 2015, **154**, 190-196.
 18. G. Schlichthorl, S. Y. Huang, J. Sprague and A. J. Frank, *Journal of Physical Chemistry B*, 1997, **101**, 8141-8155.
 19. G. Li, K. Hu, C. Yi, K. L. Knappenberger, G. J. Meyer, S. I. Gorelsky and M. Shatruk, *The Journal of Physical Chemistry C*, 2013, **117**, 17399-17411.
 20. G. Boschloo, H. Lindström, E. Magnusson, A. Holmberg and A. Hagfeldt, *Journal of Photochemistry and Photobiology A: Chemistry*, 2002, **148**, 11-15.
 21. G. Boschloo and A. Hagfeldt, *Chemical Physics Letters*, 2003, **370**, 381-386.
 22. K. Wijeratne, J. Akilavasan, A. Alamoud and J. Bandara, *Transaction on Electron Optics*, 2015, **1**.
 23. H. Kusama and H. Arakawa, *Journal of Photochemistry and Photobiology a-Chemistry*, 2004, **162**, 441-448.
 24. A. Kay and M. Gratzel, *Journal of Physical Chemistry*, 1993, **97**, 6272-6277.
 25. H. Kusama, H. Orita and H. Sugihara, *Langmuir*, 2008, **24**, 4411-4419.
 26. A. Fischer, H. Pettersson, A. Hagfeldt, G. Boschloo, L. Kloo and M. Gorlov, *Solar Energy Materials and Solar Cells*, 2007, **91**, 1062-1065.
 27. F. Nour-Mohammadi, H. T. Nguyen, G. Boschloo and T. Lund, *Journal of Photochemistry and Photobiology A: Chemistry*, 2007, **187**, 348-355.
 28. J. Wu, Z. Lan, J. Lin, M. Huang, Y. Huang, L. Fan and G. Luo, *Chemical Reviews*, 2015.
 29. H. Ng, S. Ramesh and K. Ramesh, *Electrochimica Acta*, 2015.
 30. F. Fabregat-Santiago, J. Bisquert, E. Palomares, L. Otero, D. B. Kuang, S. M. Zakeeruddin and M. Gratzel, *J. Phys. Chem. C*, 2007, **111**, 6550-6560.
 31. P. Wang, S. M. Zakeeruddin, J. E. Moser and M. Gratzel, *Journal of Physical Chemistry B*, 2003, **107**, 13280-13285.
 32. L. H. Hu, S. Y. Dai and K. J. Wang, *Acta Physica Sinica*, 2003, **52**, 2135-2139.
 33. R. V. Siriwardane and J. M. Cook, *Journal of Colloid and Interface Science*, 1986, **114**, 525-535.
 34. V. Swamy, A. Kuznetsov, L. S. Dubrovinsky, R. A. Caruso, D. G. Shchukin and B. C. Muddle, *Physical Review B*, 2005, **71**, 184302.
 35. X. Chen and S. S. Mao, *Chemical reviews*, 2007, **107**, 2891-2959.
 36. D. Lin-Vien, N. B. Colthup, W. G. Fateley and J. G. Grasselli, *The handbook of infrared and Raman characteristic frequencies of organic molecules*, Elsevier, 1991.
 37. T. Moumene, E. H. Belarbi, B. Haddad, D. Villemin, O. Abbas, B. Khelifa and S. Bresson, *Journal of Molecular Structure*, 2015, **1083**, 179-186.
 38. Y. Fan and C. J. Cornelius, *Journal of Materials Science*, 2013, **48**, 1153-1161.
 39. E. Y. Jung, B. Chae, S. J. Kwon, H. C. Kim and S. W. Lee, *Solid State Ionics*, 2012, **216**, 95-99.
 40. S. J. Hug, *Journal of Colloid and Interface Science*, **188**, 415-422.
 41. X. D. Gao and J. Chorover, *Environ Chem*, 2012, **9**, 148-157.
 42. K. D. Dobson, A. D. Roddick-Lanzilotta and A. J. McQuillan, *Vibrational Spectroscopy*, 2000, **24**, 287-295.
 43. J. R. Jennings and Q. Wang, *The Journal of Physical Chemistry C*, 2009, **114**, 1715-1724.
 44. K. M. Son, M. G. Kang, R. Vittal, J. Lee and K.-J. Kim, *Journal of applied electrochemistry*, 2008, **38**, 1647-1652.
 45. M. Doring, E. Uhlig, V. I. Nefedov and I. V. Salyn, *Z. Anorg. Allg. Chem.*, 1988, **563**, 105-115.
 46. L. B.J., H. K., J. G., G. U., F. A., N. C. and S. K., *Physica Scripta*, 1970, **1**, 286-298.

47. K. E. Lee, M. A. Gomez, S. Elouatik and G. P. Demopoulos, *Langmuir*, 2010, **26**, 9575-9583.
48. C. Bauer, G. Boschloo, E. Mukhtar and A. Hagfeldt, *The Journal of Physical Chemistry B*, 2002, **106**, 12693-12704.
49. Y. Park, Y. Mee Jung, S. Sarker, J.-J. Lee, Y. Lee, K. Lee, J. Jin Oh and S.-W. Joo, *Solar Energy Materials and Solar Cells*, 2010, **94**, 857-864.
50. M. K. Nazeeruddin, R. Humphry-Baker, P. Liska and M. Grätzel, *The Journal of Physical Chemistry B*, 2003, **107**, 8981-8987.
51. W. Q. Liu, L. H. Hu, S. Y. Dai, L. Guo, N. Q. Jiang and D. Kou, *Electrochim. Acta*, 2010, **55**, 2338-2343.
52. L. M. Peter, *Physical Chemistry Chemical Physics*, 2007, **9**, 2630-2642.
53. F. Fabregat-Santiago, J. Bisquert, G. Garcia-Belmonte, G. Boschloo and A. Hagfeldt, *Solar Energy Materials and Solar Cells*, 2005, **87**, 117-131.
54. J. Bisquert, *Phys. Chem. Chem. Phys.*, 2003, **5**, 5360-5364.
55. J. Bisquert and G. Garcia-Belmonte, *Russ. J. Electrochem.*, 2004, **40**, 352-358.
56. Q. Wang, S. Ito, M. Gratzel, F. Fabregat-Santiago, I. Mora-Sero, J. Bisquert, T. Bessho and H. Imai, *J. Phys. Chem. B*, 2006, **110**, 25210-25221.
57. J. Bisquert, D. Cahen, G. Hodes, S. Ruhle and A. Zaban, *J. Phys. Chem. B*, 2004, **108**, 8106-8118.
58. L. M. Peter, *J. Phys. Chem. C*, 2007, **111**, 6601-6612.
59. Q. Wang, Z. Zhang, S. M. Zakeeruddin and M. Gratzel, *Journal of Physical Chemistry C*, 2008, **112**, 7084-7092.
60. Y. Liu, A. Hagfeldt, X. R. Xiao and S. E. Lindquist, *Solar Energy Materials and Solar Cells*, 1998, **55**, 267-281.
61. L. Dloczik, O. Ieperuma, I. Lauermann, L. M. Peter, E. A. Ponomarev, G. Redmond, N. J. Shaw and I. Uhlendorf, *Journal of Physical Chemistry B*, 1997, **101**, 10281-10289.
62. L. M. Peter and K. G. U. Wijayantha, *Electrochimica Acta*, 2000, **45**, 4543-4551.
63. J. van de Lagemaat and A. J. Frank, *Journal of Physical Chemistry B*, 2001, **105**, 11194-11205.
64. H. Alarcon, G. Boschloo, P. Mendoza, J. L. Solis and A. Hagfeldt, *Journal of Physical Chemistry B*, 2005, **109**, 18483-18490.
65. J. van de Lagemaat and A. J. Frank, *Journal of Physical Chemistry B*, 2000, **104**, 4292-4294.
66. Z. P. Zhang, S. M. Zakeeruddin, B. C. O'Regan, R. Humphry-Baker and M. Gratzel, *Journal of Physical Chemistry B*, 2005, **109**, 21818-21824.
67. N. Kopidakis, K. D. Benkstein, J. van de Lagemaat and A. J. Frank, *The Journal of Physical Chemistry B*, 2003, **107**, 11307-11315.
68. J. Bisquert, *J. Phys. Chem. B*, 2002, **106**, 325-333.
69. R. Kern, R. Sastrawan, J. Ferber, R. Stangl and J. Luther, *Electrochim. Acta*, 2002, **47**, 4213-4225.
70. D. B. Kuang, P. Wang, S. Ito, S. M. Zakeeruddin and M. Gratzel, *J. Am. Chem. Soc.*, 2006, **128**, 7732-7733.